HAL
open science

The fixtureless inspection of flexible parts based on semi-geodesic distance

Kaveh Babanezhad, Gilles Foucault, Vahid Sabri, Antoine S. Tahan, Jean Bigeon

To cite this version:

Kaveh Babanezhad, Gilles Foucault, Vahid Sabri, Antoine S. Tahan, Jean Bigeon. The fixtureless inspection of flexible parts based on semi-geodesic distance. Precision Engineering, 2019, 59, pp.174-184. 10.1016/j.precisioneng.2019.07.002 . hal-02187215

HAL Id: hal-02187215

https://hal.science/hal-02187215

Submitted on 17 Jul 2019

HAL is a multi-disciplinary open access archive for the deposit and dissemination of scientific research documents, whether they are published or not. The documents may come from teaching and research institutions in France or abroad, or from public or private research centers.

L'archive ouverte pluridisciplinaire **HAL**, est destinée au dépôt et à la diffusion de documents scientifiques de niveau recherche, publiés ou non, émanant des établissements d'enseignement et de recherche français ou étrangers, des laboratoires publics ou privés.

The Fixtureless Inspection of Flexible Parts Based on Semi-Geodesic Distance

Kaveh Babanezhad[a,*], Gilles Foucault[a,*], Vahid Sabri[b], Antoine Tahan[b], Jean Bigeon[a]

[a]*Univ. Grenoble Alpes, CNRS, Grenoble INP, G-SCOP, F-38000 Grenoble, France*
[b]*Ecole de Technologie Superieure, 1100 Notre-Dame West, Montreal H3C 1K3, Canada*
** Corresponding Author(s)*

kaveh.babanezhad@univ-grenoble-alpes.fr

gilles.foucault@univ-grenoble-alpes.fr

vahid.sabri.1@ens.etsmtl.ca

antoine.tahan@etsmtl.ca

jean.bigeon@grenoble-inp.fr

Abstract

Some types of manufactured parts like sheet metals and skins often have a significantly different shape in a free-state position compared to their state-of-use position (as defined by their nominal CAD models) due to a combination of gravity and/or the residual effects of stress. Traditionally known as flexible (nonrigid compliant) parts, these dedicated fixtures are used for inspection operations in order to maintain flexible parts from a free-state position to a state-of-use position. This paper introduces a new automatic defect identification method primarily intended for two less-investigated manufacturing defect types: contour profile errors and hole localization. By combining simple techniques such as mesh boundary detection, fast boundary-based correspondence searches and accurate fast marching on triangulated meshes, the semi-geodesic distances from each boundary vertex on the acquired SCAN mesh to all the other boundary vertices is calculated, stored in a table and then compared to the corresponding values on the part's nominal CAD mesh. The comparisons found in the tables result in an estimation of the location and amplitude of the two aforementioned defect types. Compared to other work in this field, the overall approach does not rely on any mesh registration or finite-element analysis with tedious boundary conditions setup. It is also relatively fast. A fast algorithm/app based on this method was named the AFDA (Automatic Free-state Defect Approximation) and was validated against case studies in the aerospace sector. The results reflect the utility and effectiveness of the proposed approach.

Keywords: Metrology; Fixture; Inspection; Nonrigid; Flexible; Compliant

1 Introduction

Manufactured mechanical parts often contain geometrical differences compared to their nominal Computer-Aided Design (CAD) models and need to pass geometrical inspection during the Quality Control (QC) phase to ensure that differences are within pre-defined tolerance ranges. For rigid parts, this inspection is performed in two steps. First, there is the data acquisition in a free-state position (contact-based or non-contact acquisition, usually exported in a standard point cloud or triangular surface mesh file format). Second, there is the processing of the acquired data using Computer-Aided Inspection (CAI) tools to identify the location and amplitude of a number of manufacturing defects (depending on pre-defined tolerance types and tolerance ranges). This dual inspection routine is currently limited to parts that are only reasonably rigid. This focus on rigidity exists due to conventional CAI software requirements where it is assumed by default that any acquisition data imported to the software is from a rigid part and thus any deviation (outside typical measurement noise amplitudes) between the imported data and the nominal CAD model should be treated as a potential manufacturing defect.

The dimensional and geometrical inspection of flexible parts (also called *nonrigid* or *compliant* parts) has an additional initial step. Flexible parts such as parts with thin walls have a considerably different shape in a free-state position compared to their nominal CAD models due to the effects of gravity and residual stress remaining from the manufacturing processes. This geometric deviation is mostly due to elastic deformations rather than actual manufacturing defects. As a result, one is typically required to first set up standard or specialized conformation fixtures that will maintain the part in its state-of-use position, defined in its corresponding nominal CAD model. The state-of-use position (or ideal assembly position) is the position in which a part is conformed via fixation devices in order to maintain a shape equal to the one devised in the part's nominal CAD model. It is only after this initial step that the preliminary geometric data of a flexible part may be gathered and subsequently analyzed in conventional CAI software as if it were from a rigid part.

Multiple downsides exist in using fixtures: a time-consuming set-up process (e.g., 60+ hours for a skin panel in the aerospace industry), considerable purchase and operational expenses, limitations of standard fixtures in certain scenarios, significant errors in CAI defect identification if the fixation has not been conducted correctly (since conventional CAI tools are designed and fine-tuned for rigid parts only) etc. Such disadvantages have led researchers to try to circumvent the use of fixtures in the inspection of flexible parts. They achieved this by:

1) Digitally deforming (better known as *registering*) the gathered point cloud/mesh data of a flexible part in a Euclidean space until it superimposes onto the part's corresponding nominal CAD model, thereby elastically deforming the data to obtain an optimal assembly shape while avoiding the neutralization of any existing manufacturing defects. This registration is referred to in this paper as a ***flexible registration***.
2) Importing the superimposed point cloud/mesh data into conventional CAI software (or custom-made tools resembling them) for defect identification purposes. This defect identification is referred to in this paper as a ***complementary defect identification***.

Our work aims at the identification of contour profile and hole localization defects defined in the ISO-1101:2012 Geometrical Product Specifications (GPS) standard (or its equivalent, e.g., the ASME-Y14.5:2009) as all-over specifications without datum referencing.

(1) Hole (Center) Localization
under Position [⌖]
(Position Tolerance, GPS Sub-clause 18.12)

(2) Contour Profile Error
under 3D Profile Line [⌒]
(Form Tolerance, GPS Sub-clause 18.5)

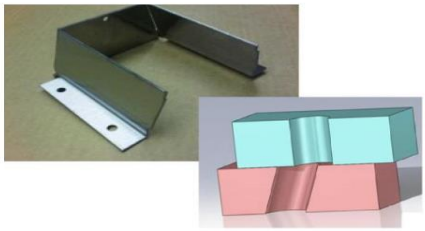

(courtesy of GeometricGlobal.com)

(courtesy of Team-bhp.com)

Fig. 1 - Common manufacturing defects in flexible parts

The aforementioned two-fold fixtureless inspection approach for flexible parts (flexible registration + complementary defect identification) possesses its own disadvantages, most notably: (1) dependence on a near-perfect prior flexible registration (which is not guaranteed to be achievable) and low potential accuracy in complementary defect identification without such a near-perfect flexible registration; (2) typically high runtimes of flexible registration methods.

This paper aims to investigate whether a defect identification method that does not necessarily rely on a prior flexible registration could be introduced or not. By the end of this study, it was demonstrated that the answer to this hypothesis is 'Yes'. A novel method was proposed to identify the location and amplitude of manufacturing defects with a predetermined level of confidence. The algorithm developed based upon the proposed method was named the AFDA. The acronym stands for the Automatic Free-state Defect Approximation algorithm. Resulting contributions of this paper advance the state of the art under various metrics including automation, runtime, precision (repeatability of the numerical process and robustness) and interoperability. Compared to other work in this field, the overall approach does not need mesh registration, avoids the use of finite-element analysis with tedious boundary conditions setup and is relatively fast.

The remainder of this paper is organized as follows: A review of the state of the art is found in Section 2. The proposed method is presented in Section 3. The validation approach (including assumptions and uncertainties) is explained in Section 4.1, while the obtained results are presented in Section 4.2. A discussion on interpreting the results and future work is available in Section 5. Concluding remarks (including a detailed synthesis of the contributions) are available in Section 6.

2 Literature Review

A summary of the recent advances and research trends in the field (the fixtureless inspection of flexible parts) are well detailed in [1] and accompanied by the specific definitions, notions and challenges of dealing with flexible parts. The notion of flexibility, however, was first quantified in [2]. Almost the entire body of previous research work in the field can be considered under three-part taxonomy:

1) **Flexible Registration (with Complementary Defect Identification)**: A flexible registration method is effectively a modified nonrigid point set registration method that respects intrinsic (dimensional and shape) properties of the part during the registration of the acquisition data towards the nominal CAD (in order to avoid the suppression of any existing defects in the data or creating new artificial ones). Typically, these methods try to find a nonrigid registration that minimizes the Euclidian distance between the acquisition data (or SCAN) and the nominal CAD while respecting some criteria related to the intrinsic (dimensional & shape) properties of the part. The nonrigid point set registration performed within a flexible registration method can be based on a Finite Element Analysis (FEA) [3-14] or based on a probability density estimation [16-17]. As a result, a flexible registration

operation is either FEA-based or probabilistic. The FEA-based flexible registration methods often have significant runtimes, while probabilistic ones have managed to reduce runtimes to some degree. As an added bonus, most flexible registration methods also attempt to identify the location and amplitude of manufacturing defects by displaying a colormap of distances between the registered acquisition data and the nominal CAD. This colormap, whose outliers are considered to be manufacturing defects, may result in accurate defect identification only if a near-perfect flexible registration is achievable. This use of a colormap of distances after a flexible registration is referred to in this paper as complementary defect identification. It could be said that various such methods exist based on how the distances are calculated after registration. For example, the complementary defect identification in [18] is based on a projected point-to-point distance calculation, while the one in [16] is based on a point-to-point distance calculation and the one in [17] is based on point-to-triangle and point-to-line distance calculations.

2) **Defect Identification**: In contrast to complementary defect identification methods, an impartial method does not rely on a prior flexible registration operation. Despite recent developments in probabilistic flexible registration [17], there is still no guarantee that a near-perfect flexible registration is possible (due to unavoidable uncertainties in real-world scenarios). As mentioned earlier, most flexible registration methods still possess high runtimes. Thus, a standalone defect identification is theoretically superior to a complimentary one. The method of [2], named IDB-CTB, calculates curvature information (Gaussian and mean curvature) for each vertex of the acquisition data (or SCAN) captured from the part in free-state position. This information is then deducted from equivalent curvature information on corresponding vertices on the nominal CAD. By applying the Thompson extreme value statistical test [19] and the bi-weight mean and standard deviation estimator technique [20] on the resulting deduction, the IDB-CTB manages to identify two types of manufacturing defects (dent shapes and waviness, see Fig. 1). In [15], the use of arc length has been proposed as a method to identify two types of manufacturing defects (hole localization and contour profile error). Traditionally, measurement tapes were used during geometrical inspections to measure the geodesic distances between functional features (e.g. tooling hole, circumference). The authors propose to perform numerically similar geodesic measurements on CAD and SCAN in a digital environment. In this approach, pre-defined vertices of interest (e.g., datum points, corners, hole centers, etc.) are first selected on a CAD. By applying an implementation of the Fast Marching Method (FMM) [21] on a CAD, a matrix of all shortest geodesic paths between each pair of selected vertices of the CAD is obtained. A FMM is then also applied to SCAN for the vertices visually corresponding to the ones previously selected on the CAD, subsequently resulting in another matrix containing all shortest geodesic paths between each pair of the selected vertices of SCAN. The differences between the distances recorded in the two matrices represents the difference metrics on the SCAN, therefore considered as a manufacturing defect when its amplitude is greater than the overall tolerance.

3) **Assembly Assessment**: Assembly assessment methods are concerned with verifying the state of a flexible part in an assembly. They are typically performed after complementary defect identification has concluded. Their role is to predict various consequences like the optimal assembly sequence and its effects on the final shape of a flexible part in an assembly [22], the post-assembly shape of a flexible part under normal lighting conditions [23], or the required assembly boundary conditions to insure a post-assembly shape that closely resembles the nominal CAD [24].

3 Methodology

Definitions:

The Euclidian distance is the straight line distance between two points A and B in the Euclidian space.

Geodesic distance: Let S be the surface of the part, and $\{C(A,B)\}$ be the set of curves on S connecting two points A and B on S. The geodesic distance between points A and B on S is the length of the shortest curve in $\{C(A,B)\}.)\}$. In the context of triangular meshes, we use "semi-geodesic distance" term as the FMM method approximates the length of the shortest curves from a given boundary vertex to all other boundary vertices of the mesh.

Difference: Algebraic difference between the geodesic distances on the nominal model (as defined in the CAD) and geodesic distances observed on the measured part (as defined in the SCAN).

Fig 2: the handheld optical 3D Scanner "MetraSCAN" from Creaform was used to generate the SCAN mesh

The process starts with the generation of the SCAN mesh. The SCAN point cloud is acquired by scanning the displaced part using a contactless measuring system such as optical scanning. In our work, we used the handheld optical CMM MetraSCAN 3D (Creaform), featuring an accuracy up to 0.030 mm and a resolution of up to 0.050 mm (See Fig 2).

The SCAN mesh is generated with the Delaunay triangulation of the point cloud.

The main idea of our defect identification method is that geodesic distances are preserved on compliant parts where stretching has marginal effects (compared to bending and twisting/torsion effects). The underlying concepts behind the method are summarized in Fig. 2. After a rigid pre-alignment of the SCAN mesh and CAD nominal model using ICP method [25], the nominal CAD model is meshed using the constrained Delaunay method [26], where boundary vertices are aligned with the SCAN ones, respecting the same mesh size with the corresponding list of matching boundary vertices. Afterwards, a Fast Marching Method (FMM) calculates geodesic distances from any boundary vertex to other boundary vertices on both meshes [27]. For each pair of CAD-SCAN matching vertices, the distance difference vector is calculated on CAD and SCAN meshes, called FGD_C and FGD_S, and an outlier detection method in the differences of FGD_C and FGD_S is used to identify the amplitude and the localization of defects.

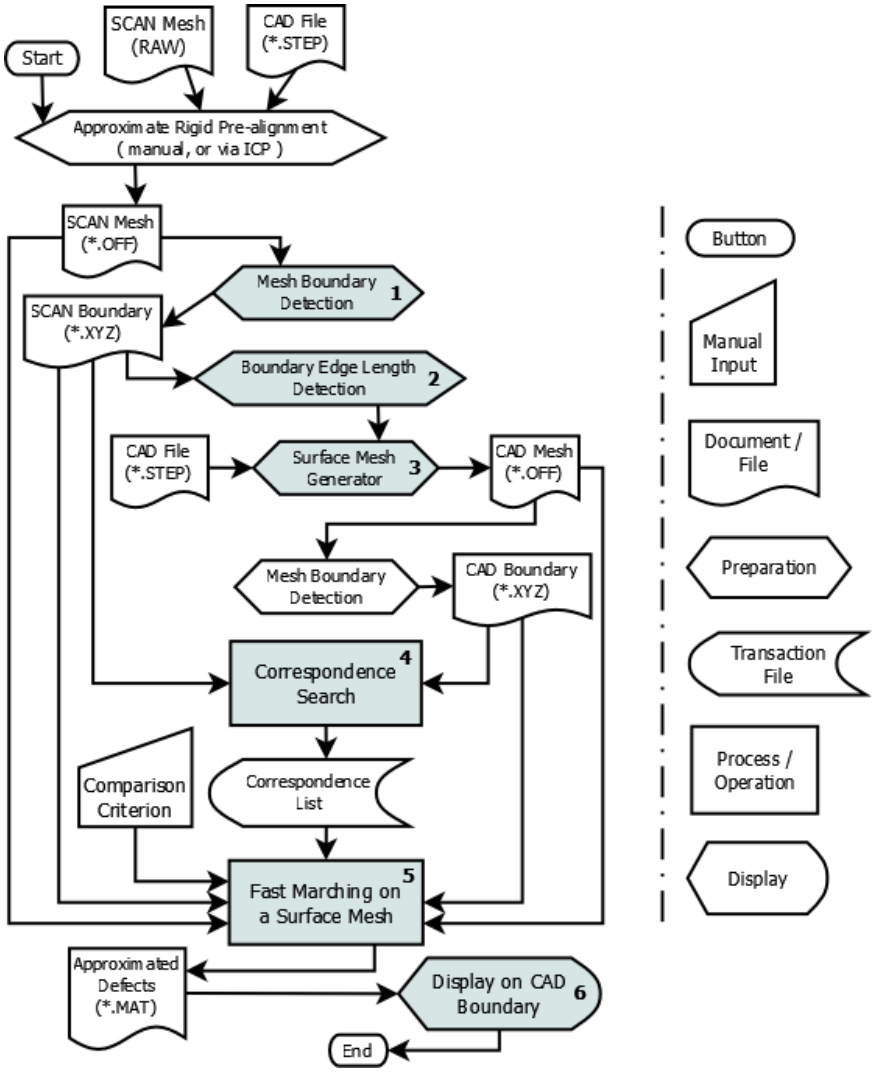

*.OFF is a surface mesh file format & *.XYZ is a point cloud file format.
*.STEP is a file format for representing 3D objects in CAD software based on ISO 10303-21 standard.
*.MAT is a binary data container format that the MATLAB®

Fig. 3 – Main steps of the proposed (AFDA) method

In step 2 (Fig 3), boundaries of the SCAN mesh are identified by selecting edges with a single adjacent triangle. The CAD mesh generation starts by creating the set of mesh vertices superimposed on CAD vertices. Then, CAD boundary edges are meshed using the same mesh size as the SCAN boundary mesh. As a result, CAD and SCAN boundary meshes contain the same number of vertices, each matching one vertex of the other mesh. The CAD surface is meshed with the constrained Delaunay method initialized from its boundary mesh. This overall method generates a CAD triangulation close to the SCAN mesh Euclidian projection.

In step 3 of the method, the FMM Sethian (1995) calculates the shortest semi-geodesic distance (path) from a given boundary vertex to all other mesh vertices (Fig 4). Our method initiates the FMM distance calculation for the k boundary vertices of a CAD mesh. Distances are stored into the FGD_C matrix of size $k \times k$ containing all the geodesic distances from each boundary vertex to the k other with the square symmetrical form described below:

$$FGD_C = \begin{bmatrix} 0 & d_{12} & d_{13} & \dots & d_{1k} \\ d_{21} & 0 & d_{23} & \dots & d_{2k} \\ d_{31} & d_{32} & 0 & \dots & d_{3k} \\ \dots & \dots & \dots & \dots & \dots \\ d_{k1} & d_{k2} & d_{k3} & \dots & 0 \end{bmatrix}_{k \times k} \qquad \textbf{Eq. 1}$$

where d_{ij} represents the *shortest* semi-geodesic distance between the ith and the jth boundary vertices on the CAD mesh ($d_{ij} = d_{ji}$ and $d_{ii} = 0$). A similar matrix FGD_S of size $k \times k$ is also obtained after applying the FMM method on the SCAN mesh, where boundary vertices are renumbered in such a way that the ith vertex of the SCAN mesh corresponds to the ith vertex of the CAD mesh.

The absolute differences between the corresponding distances in FGD_C and FGD_S is then considered a measure for approximating existing manufacturing defects, respectively defined as:

$$\Delta_F = |FGD_S - FGD_C| \qquad \textbf{Eq. 2}$$

where Δ_F is of the same $k \times k$ size, and its ith row (or column) represents a geodesic deviation measure for manufacturing defects from the point of view of the ith boundary vertex on the CAD mesh. This measure is used to calculate comparison criteria for the identification of contour profile errors for rectilinear boundaries and hole center localization for circles. While the comparison can be made with any vertex manually selected, two automatic comparison scenarios are given for comparison criteria:

1) **Entire Boundary Detection**: the entire boundary of the CAD mesh could be used as a comparison criterion. In this context, the average of each row (or column) of Δ_F will be picked as an estimation of defect amplitude for the vertex corresponding to that row (or column) from the point of view of all the other vertices. The result of this operation would be a vector of $k \times 1$ size (or $1 \times k$), representing approximate defect amplitudes for each boundary vertex. Given the assumption stating that defect regions does not cover the majority the part, considering the average of each row (or column) will reduce the effects of other vertices on the CAD/SCAN boundary that might already be in a defect zone and will focus the approximation on the vertex represented by that row (or column).
2) **Border Selection**: Defining the border as the biggest loop on the boundary of the CAD mesh and choosing the border as a comparison criterion has all the advantages of scenario #1 and allows for a precise evaluation of the holes' inner loop localization. The concept of connected components (from graph theory) was used to determine separate loops (components) of the CAD boundary. In practice, finding the connected components is actually quite straightforward by using either the Breadth-first search (BFS) [28] or the Depth-first search (DFS) [29] algorithms. Next, the length of each loop was calculated via the sum of the Euclidean lengths of all the edges in each loop. The remainder of the procedure for using border vertices is similar to scenario #1.

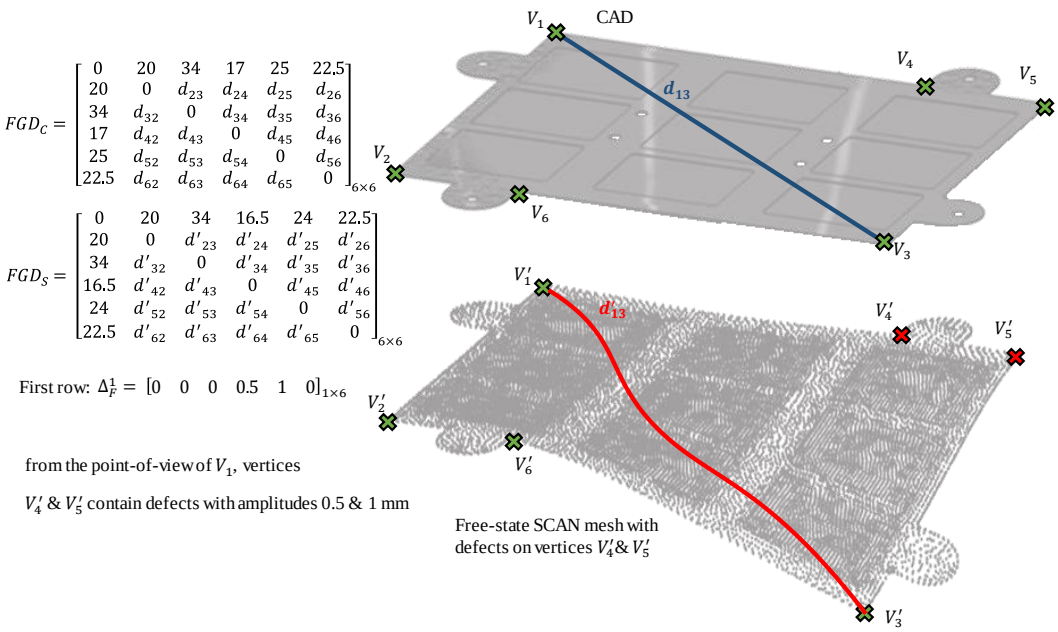

Fig. 4 – Simplified example solved by the AFDA methodology

Step 4 of the overall algorithm entails the mechanism required to display and clarify the location of any existing manufacturing defect. The amplitude for any (potential) manufacturing defect has already been calculated in step 3: Δ_F. In fact, in step 3, all the vertices residing on the boundary of the part are considered to be potentially in a defect region (and an amplitude is assigned to them). Now, using the assigned amplitudes, the intent is to clarify which of the vertices are in a defect region. This can be done either via an interaction with the end-user or automatically.

Traditionally, once an algorithm has converged to its results, a colormap (often depicted on the nominal CAD or free state SCAN) displays the calculated amplitude for each vertex of the acquisition data. Such an amplitude could be the distance difference between each vertex of the registered SCAN mesh and its corresponding vertex on the nominal CAD mesh. The disadvantage of this approach is the need for a final interaction with the end-user, thus no autonomous implementation for production lines. The advantage, however, is that a human operator would be a lot better at interpreting the colormap compared to a computer heuristic. Alternatively, outlier detection methods such as the Grubb's test [30] or GESD test [31] could be applied to a set composed of the amplitudes for all vertices. The detected outliers of this set are then introduced to the end-user as vertices residing in defect regions. The disadvantage of this approach are the false positives (vertices not in defect regions mistakenly detected as belonging to one) whereas the advantage is in the automation. Applications of both of these approaches on one of the case studies used in validation of the AFDA are depicted in Fig 5.

(1) Interactive Display via a Traditional Colormap

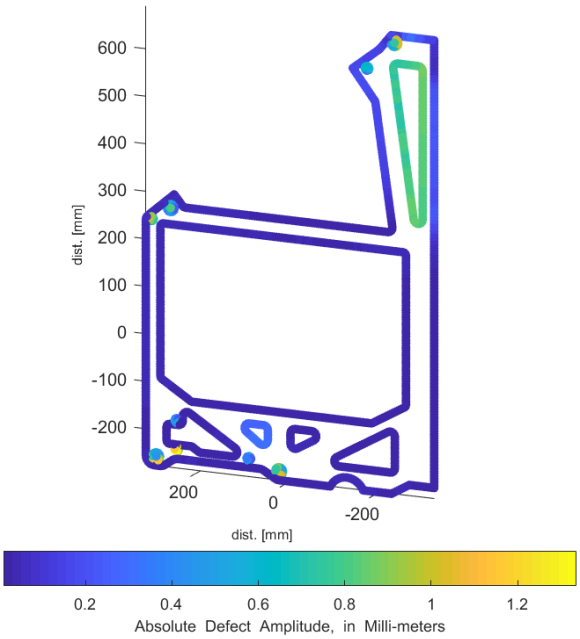

(2.1) Auto. Display via Tolerance Ranges of the Part

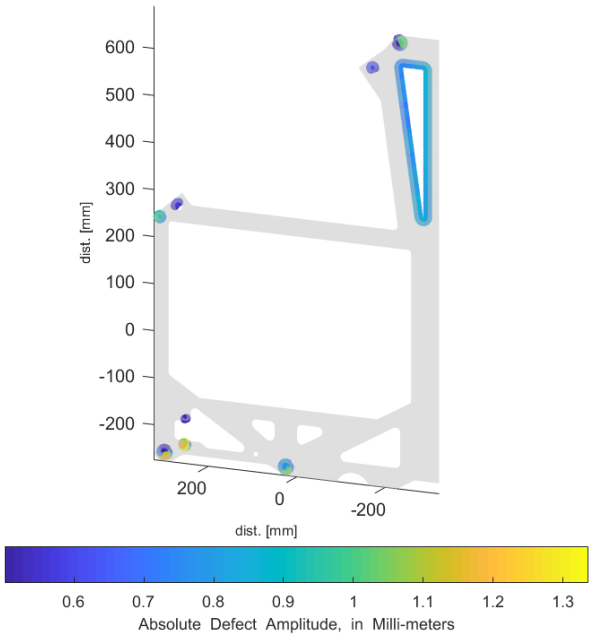

(2.2) Auto. Display via Grubbs' Test [30]

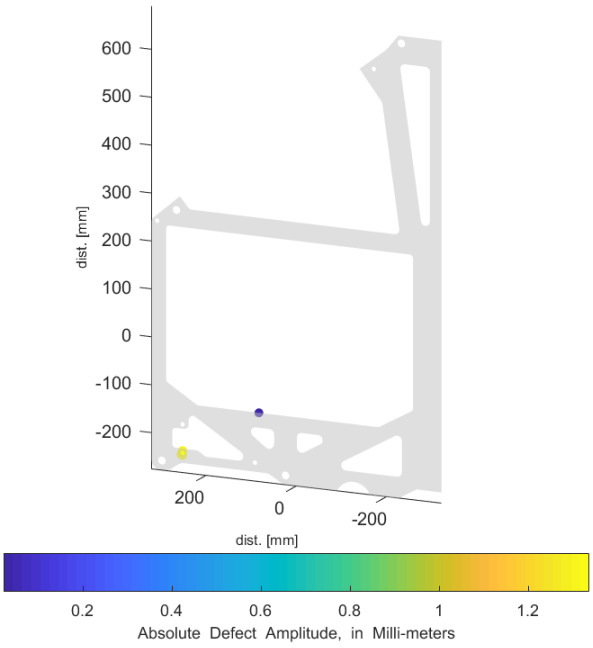

(2.3) Auto. Display via GESD Test [31]

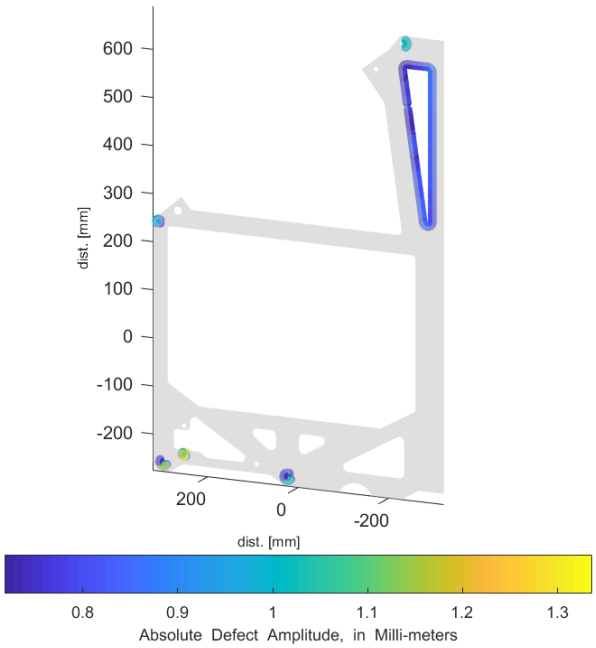

Fig. 5 –Examples of identified defects in the AFDA

4 Results

4.1 Validation Approach

This study follows a case study based approach for examining its hypothesis. An investigation of the claims of the proposition are therefore performed by validating the AFDA against a virtual (simulated) case study on a typical part under various comparison criteria in both free-state and state-of-use positions (enabled via a hypothetical perfect flexible registration). This accounts for a total of 7

case study instances. The following sub-sections describe various aspects of the adopted validation approach.

4.1.1 Assumptions

The following assumptions were initially made in this study before validations:

(*i*) the triangulated point cloud (mesh) of the scanned part is available (containing manufacturing defects having their geometric deviation at a free-state position greater than the part's pre-defined profile tolerance ranges) is not a partial scan and has reasonably clean boundaries (imperfections below 10% of the part's overall profile tolerance range, at worst). Defects' geometric deviation at the free-state position must also be greater than the overall profile tolerance range;

(*ii*) the mesh of the scanned part has a quasi-constant density across the surface area and data acquisition equipment noise is much smaller than defect amplitudes;

(*iii*) defect areas do not cover the majority of the part and inspection is generally limited to the defects described in Fig. 1 and in accordance to the standard definition each was placed under. Specific to the methods developed in this paper, an inspection is limited to hole center localization and contour profile defects.

4.1.2 Creating Case Studies

A case study is comprised of the CAD model of an industrial part that is modified to contain a number of artificial defects and subsequently deformed under simulated gravity in finite element (FE) software resulting in a virtual SCAN in free-state position. Detailed specifics of creating a virtual case study vary based on input geometry types. In this study, the following procedure was undertaken:

1) The CAD model of an industrial part is modified to contain suitable defects (types #1 and #2 in Fig. 1). This modified version of the CAD model is then deformed using a SolidWorks® FE software package (e.g., the part is mounted on one side and deviates due to simulated gravity) and subsequently saved as a deformed solid body, acting as a virtual scan of the part in its free-state position.
2) This is followed by extracting one of the key surfaces of both the nominal CAD model and the virtual SCAN (representing the surface that would have been scanned in a real-world scenario), and exporting both surfaces in *.STEP file format.
3) Next, a surface meshing operation is applied to the extracted SCAN surface and exported in *.OFF file format. In terms of software resources, MEFISTO-MESHER (via FreeCAD®) was used for surface mesh generation.
4) The mesh generation on the extracted CAD surface happens later as per defined in step 3 of the overall method (steps #2 and #3 in Fig. 3).
5) Finally, a simulated Gaussian measurement equipment noise is added to the *.OFF mesh of the virtual SCAN (in per-vertex average normal directions).

4.1.3 Uncertainties

In creating virtual case studies, a simulated Gaussian noise (with a $\pm 3\sigma$ =25 μm) was added to the virtual SCAN meshes to account for measurement equipment noise. This Gaussian noise was obtained by moving SCAN mesh vertices $\vec{P_1}$ in their average normal direction $\overrightarrow{N(P_1)}$ with a random amplitude a having a Gaussian distribution : $\vec{P_1} = \vec{P_1} + a \cdot \overrightarrow{N(P_1)}$ and $a = \frac{1}{4}(\mathrm{Max} - \mathrm{Min})N(0,1)$ where $N(0,1)$ is the random number having a standard Gaussian distribution (mean=0, STD=1), $\mathrm{Min} = -25$ μm and $\mathrm{Max} = +25$ μm. Min and Max values are considered as the 5th and 95th percentile of the measurement noise.

The average normal direction was calculated as the average of normals at triangles F_j adjacent to vertex $\vec{P_i}$. Consequently, the average normal vector $\overrightarrow{N(P_i)}$ at vertex $\vec{P_i}$ is given by $\overrightarrow{N(P_i)} = \frac{1}{n}\sum_{j=1}^{n}\overrightarrow{N(F_j)}$ where $\overrightarrow{N(F_j)}$ is the normal vector to triangle $\boldsymbol{F_j}$.

This brings the virtually created case study closer to real acquisition data. Also, when creating case studies, during the process of creating a solid body from the deformed finite element mesh, some errors are induced in curvilinear dimensions by the finite element solver (see Fig. 6).

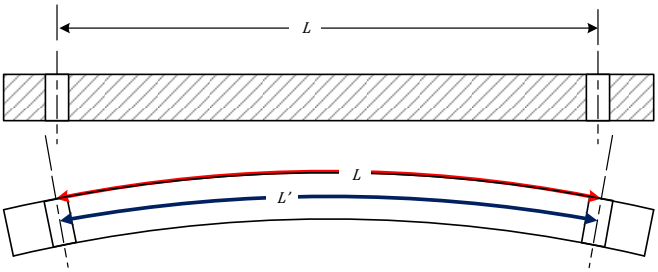

Fig. 6 – Description of curvilinear errors

4.1.4 Evaluation Metrics

The overall performance is evaluated by comparing the identified defect amplitudes at boundary vertices with the pre-defined known artificial defect amplitudes of the case study. Two evaluation metrics can be considered to describe the error in estimating the defect amplitudes via an algorithm. The first metric, a relative Metrological Algorithmic Error (MAE) is defined as follows:

$$MAE = \frac{|KDA - EDA|}{Tol} \qquad \text{Eq. 3}$$

where KDA is a vector representing known defect amplitudes for vertices of the virtual case study that contain defects, EDA is a vector representing the estimated defect amplitudes for the aforementioned vertices known to contain defects, and Tol is the overall tolerance range for the part. The MAE then becomes a vector describing the per-vertex algorithmic error relative to the overall tolerance range [16] [15]. The acceptance criteria for a measurement system, the threshold of 10% for the capability ratio of measuring system, is considered generally to be adequate by the Automotive Industry Action Group [32]. We refer the reader to for further details on the choice of this threshold [33].

With that mindset, a $MAE < 10\%$ is highly desirable, $MAE < 30\%$ is acceptable and $MAE > 30\%$ is considered unusable.

The second metric, a Statistical Algorithmic Error (SAE) is defined in Eq. 4 as follows, where KDA and EDA are the same as described in Eq. 4, and $q_{95\%}$ is the 95th percentile of the vector of absolute differences between known defect amplitudes and estimated defect amplitudes.

$$SAE = q_{95\%}\,(\,|\,KDA - EDA\,|\,) \qquad \text{Eq. 4}$$

SAE is a scalar describing a kind of worst-case scenario in which, for an algorithm, in 95% of defect estimations have their error $\leq SAE$.

4.2 Results on a virtual test case

This virtual case study uses a skin panel emanating from the aerospace industry. In this case, the profile tolerance ranges are typically between 0.8 to 1.2 mm. As a result, profile and position tolerance

ranges have been set up to 1 mm for this 965 mm long part. To simulate acquisition noise, a Gaussian noise of 25 µm amplitude was added to the virtual SCAN mesh.

Furthermore, as mentioned earlier, this case study is available in both free-state position (named F1) and state-of-use position provided by a registration to the CAD nominal shape (F2). A top view of a virtual case study (with the known defect regions emboldened in red) is depicted in Fig. 7. Similar to traditional inspection routines, the part was divided into multiple zones to set different amplitudes for hole center localization defects and contour profile errors. Actual known amplitudes of these induced defects are available in **Table 1**. Obtained results when validating the AFDA against this case study are summarized in Fig. 8 and Fig. 9.

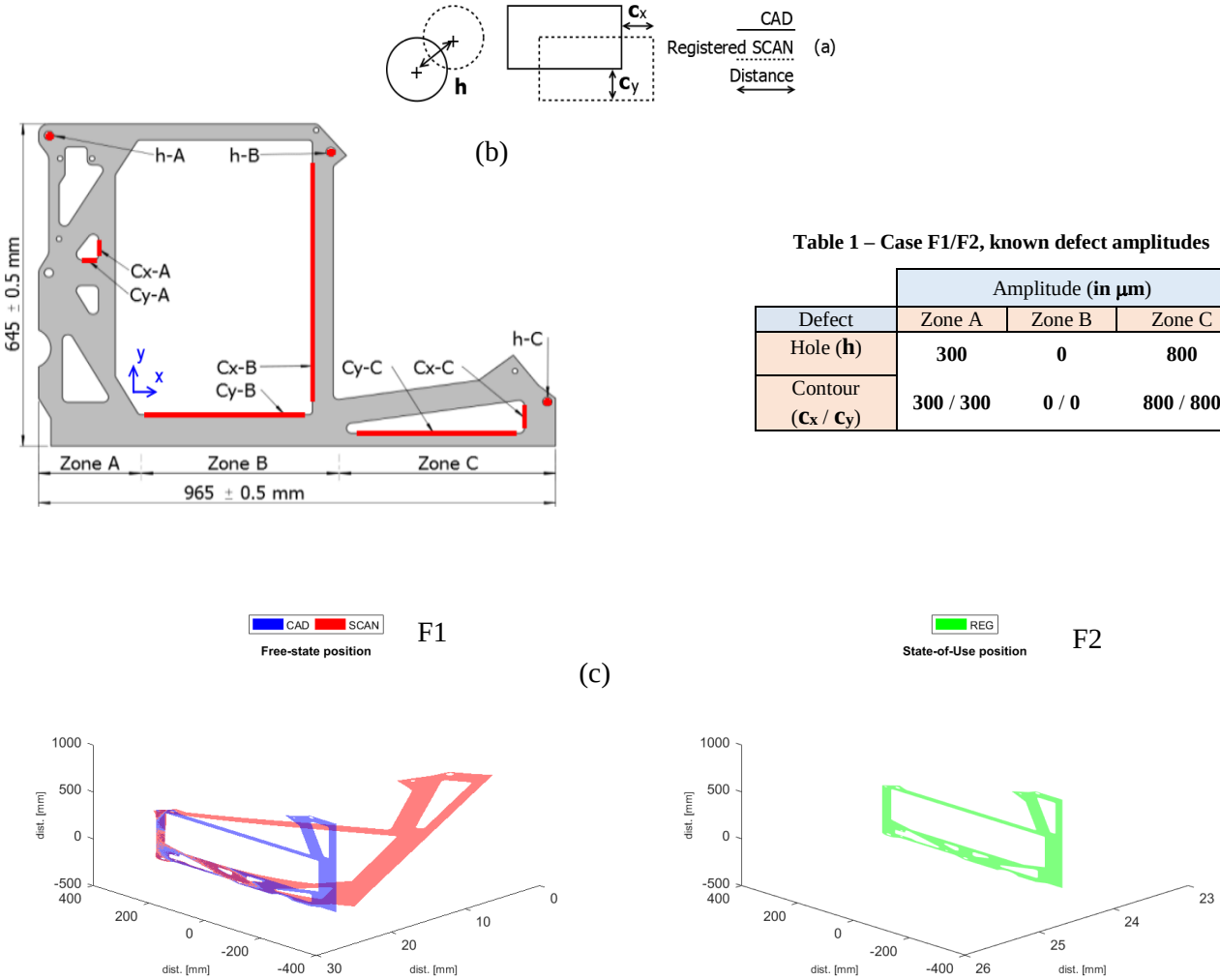

Table 1 – Case F1/F2, known defect amplitudes

	Amplitude (**in µm**)		
Defect	Zone A	Zone B	Zone C
Hole (**h**)	**300**	**0**	**800**
Contour (**c_x / c_y**)	**300 / 300**	**0 / 0**	**800 / 800**

Fig. 7 – Defects and analyzed dimensions (a) top-view of the F1/F2 case study (b) F1: free-state position case study (c) state-of-use position case study

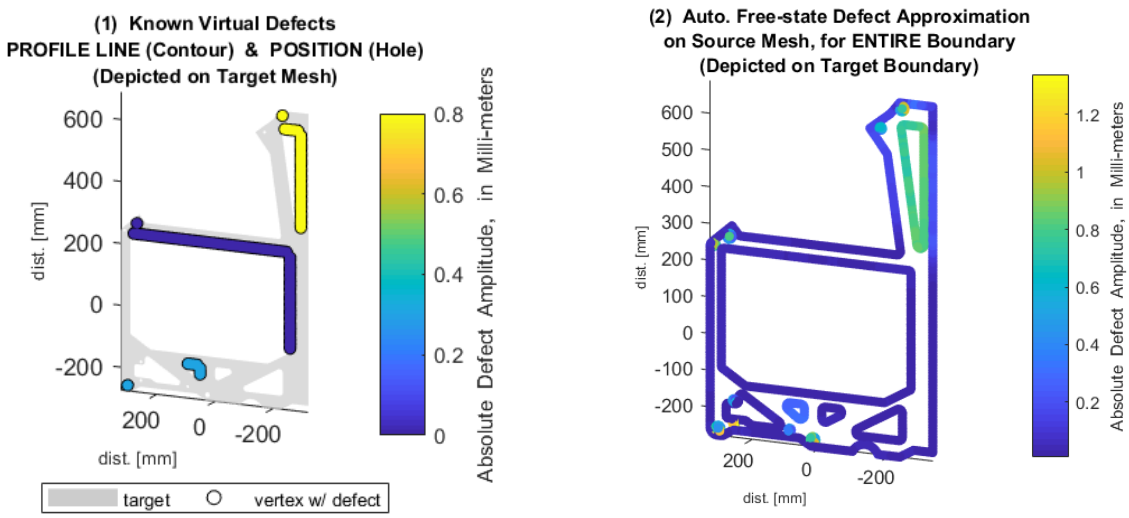

Fig. 8 – Case F1, Border selection comparison criterion

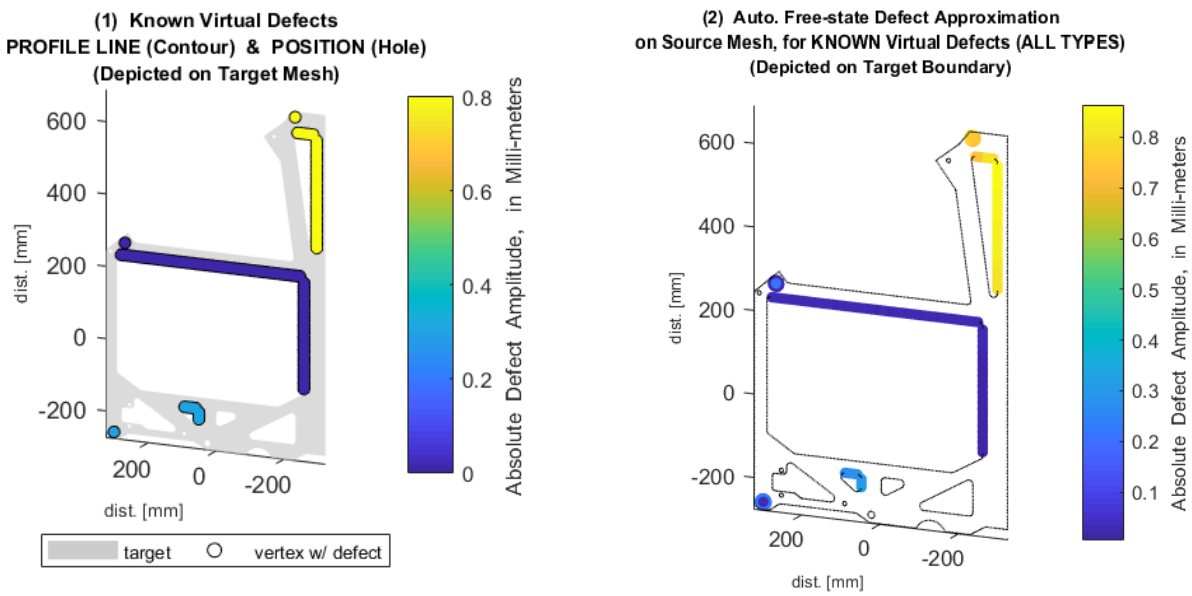

Fig. 9 – Case F2, Border selection comparison criterion

4.3 Results on an industrial test case

The proposed AFDA method was compared on an industrial case study to IDB-ACPD registration method [15] on the same case study in [15] (See Fig. 10). The case study is a sheet metal part, having four bends and two holes. Manufacturing defects were imposed in three different positions and with different values (see Fig. 10 (c)). Fifteen cases are generated with different defects combining different positions and values. We performed measurements at Free State, using the optical Metrascan scanner depicted in Fig 2 and presented in section 3. Table 2 represents these cases as well as the nominal values and the position of the imposed defects, absolute values of the estimations by the IDB-ACPD and our AFDA method, along with the Metrological Algorithmic Error percentage (MAE) knowing the overall

tolerance 4mm. In this case study, the maximum MAE value is 16% for AFDA, better than the 35% for the IDB-ACPD.

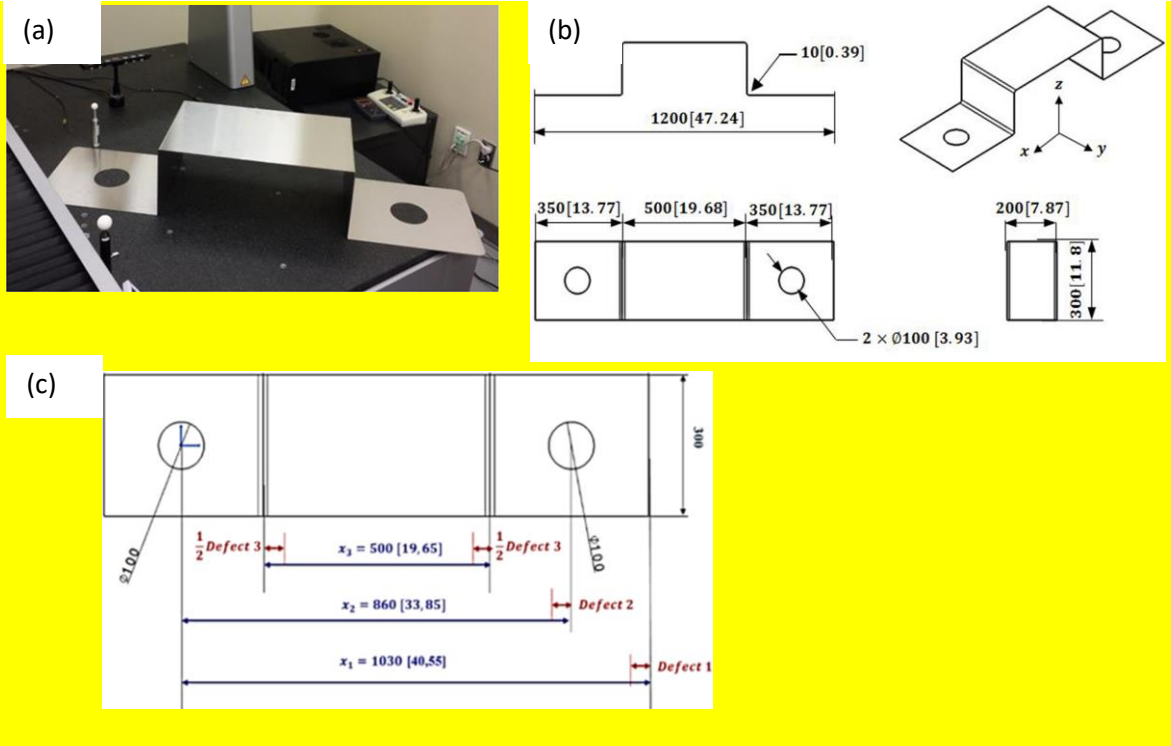

Fig. 10– Industrial case study [15]

Table 2: Case studies with the position and the nominal values of the defects, and estimated values of the defects by each method

CASE		Nominal value of defects (mm)			Estimated value of defects [mm] MAE (%)					
					IDB-ACPD [15]			AFDA		
		Δx_1	Δx_2	Δx_3	Δx_1	Δx_2	Δx_3	Δx_1	Δx_2	Δx_3
B1	V1	3.5	-	-	3.57 2%	-	-	3.79 7%	-	-
	V3	17.5	-	-	17.93 11%	-	-	17.84 9%	-	-
	V5	35	-	-	35.45 11%	-	-	35.4 10%	-	-
B2	V1	0	1.8	-	-	1.9 3%	-	-	2.17 9%	-
	V3	0	9	-	-	8.8 5%	-	-	9.34 9%	-
	V5	0	18	-	-	17.37 16%	-	-	18.35 9%	-
B3	V1	3.5	1.8	-	3.46 1%	1.17 16%	-	3.8 8%	2.02 6%	-
	V3	17.5	9	-	17.59 2%	8.37 16%	-	17.87 9%	9.3 8%	-
	V5	35	18	-	34.58 11%	17.13 22%	-	35.44 11%	18.36 9%	-
B4	V1	-	-	5	-	-	4 25%	-	-	5.6 15%
	V3	-	-	25	-	-	25.86 22%	-	-	25.57 14%
	V5	-	-	50	-	-	48.6 35%	-	-	50.54 14%
B5	V1	3.5	1.8	5	3.3 5%	1.51 7%	4.12 22%	3.75 6%	1.96 4%	5.35 9%
	V3	17.5	9	25	17.6 3%	8.35 16%	24.27 18%	17.94 11%	9.34 9%	25.64 16%
	V5	35	18	50	34.47 13%	18.61 15%	48.73 32%	35.39 10%	18.3 8%	50.07 2%

5 Discussion

All computational operations in this study were performed on a dual-core Intel Core®i5-4300U machine clocked at 1.9 GHz and equipped with 4.0 GB of RAM and a 64-bit MS Windows® operating system. The AFDA was developed in a MATLAB® (R2016a) environment and ran on a single CPU core. Noteworthy observations over the obtained results (Fig 8., Fig. 9, and Fig. 10) are as follows:

The Metrological Algorithmic Error: The MAE in defect-identified results obtained by the AFDA were below 30%. As shown in Fig 11, the algorithmic errors for a comparison criterion based on the border selection is consistently lower than the other one based on the entire boundary selection. Considering the case study error analysis in Fig 11, 91% of F1 and 100% of F2 boundary vertices respect the condition $MAE \leq 30\%$.

Statistical Algorithmic Error: Fig. summarizes the SAE from F1 and F2 cases with both comparison criteria. The same conclusions about the superiority of comparison criterion based on border selection appear true here as well.

Runtime: Case study instances converged in 60 seconds or less (Table 2). Such runtimes are significantly lower than those of other methods such as IDB-ACPD [16] (~323 second for case study F1) or BOFR-1 [17] (~230 seconds for case study F1) which require a prior flexible registration between SCAN and CAD before being able to perform defect identification operations.

The main limitation of the current implementation is the lower accuracy on hole center localization defects, and criterion based on entire boundary selection which include hole contours. These errors are related to the mismatching positions between CAD and SCAN boundary vertices on circles describing holes. Indeed, there is no imposed CAD vertex on circles to constrain the position of SCAN mesh nodes.

Overall, the proposed AFDA method is very suitable for quick checks of the dimensional and geometrical conformity.

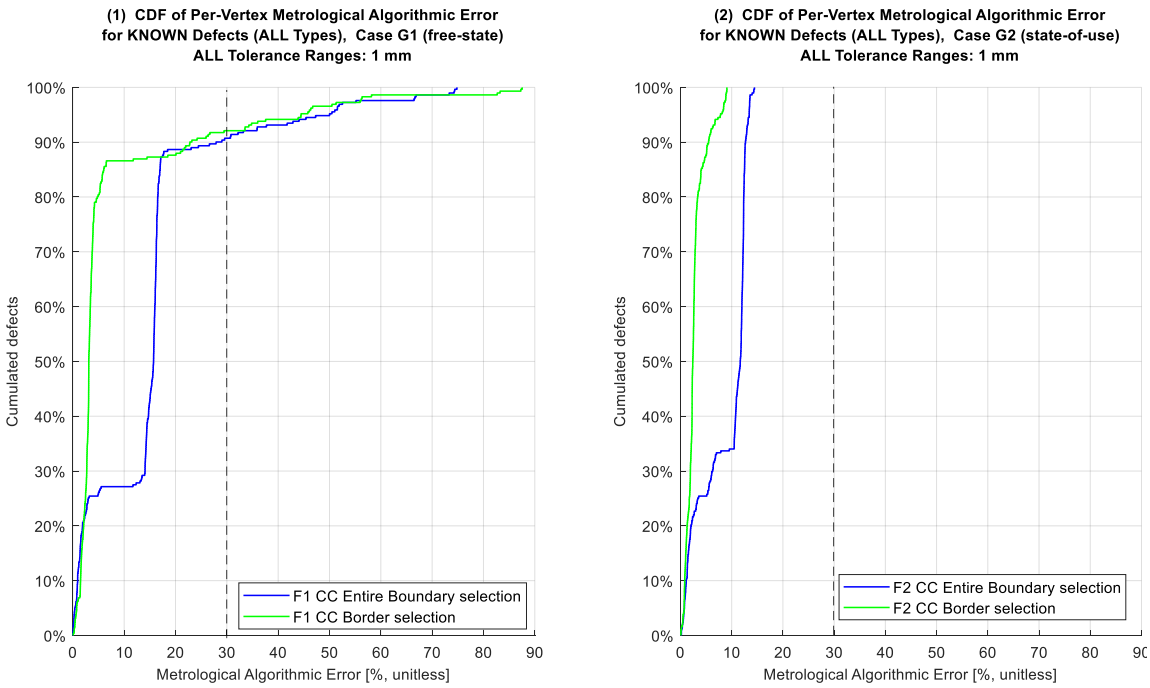

Fig. 11 – Metrological Algorithmic Error (MAE) associated with the AFDA across all case studies (F1 & F2)

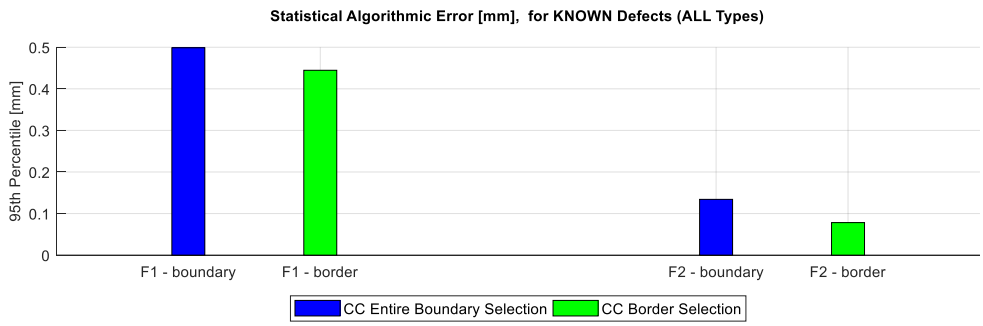

Fig. 12 – Statistical Algorithmic Error (SAE) associated with the AFDA across all case studies (F1 & F2)

Table 3 – AFDA Runtimes

Case Study		# of Vertices	# of Edges	# of Triangles	Average Boundary Edge Length [mm]	Mesh Density [vertices per cm^2]	Runtime [sec]
F1	SCAN	18348	53573	35211	4.788	11.04	55.67
	CAD	18327	53510	35169	4.788	11.03	
F2	REG	18349	53576	35213	4.788	11.04	51.56
	CAD	18327	53510	35169	4.788	11.03	

6 Conclusion

In this paper, a new defect identification methodology was proposed to deal with the problem of the fixtureless inspection of flexible parts. This is a real concern in the industry due to the various difficulties it imposes. The proposed method has advantages over other methods, such as not requiring a prior flexible registration or rigid pre-alignment, not requiring any FEA operation and being noticeably faster (when compared to a complementary defect identification approach which relies on a near-perfect prior flexible registration). An algorithm was developed and tested against multiple instances of a typical virtual industrial case study. The obtained approximations of the defect amplitudes demonstrated the potential of the approach for quality control purposes, in turn forecasting the ability to mount the parts in an assembly. Resulting contributions advance the state of the art under various metrics, which include:

Automation: The AFDA is an automatic tool which does not require user input to function. This automatic behavior also provides defect approximations on the entire contour profile of a part in one instance which can be of great industrial interest.

Runtime: The AFDA has a runtime significantly lower than fixtureless inspection methods that require prior flexible registration (e.g., probabilistic methods such as IDB-ACPD and BOFR-1, or FEM-based methods such as GNIF [9-10]). During its validation in this study, the AFDA achieved runtimes lower than 60 seconds.

Precision (repeatability): The AFDA behaves in a deterministic manner and produces the same results regardless of whether the SCAN has been rigidly pre-aligned with the CAD or not. This holds true in theory since none of the building steps of the AFDA contain any stochastic elements. This deterministic behavior actually increases the overall precision (repeatability) of the proposed method.

Interoperability: Apart from the free-state defect approximation of flexible parts, the AFDA can also be used to inspect rigid parts (in which case the approximations are even more accurate as no temporary curvilinear/geodesic errors exist in the state-of-use position). Furthermore, the approximated results obtained by the AFDA (which are calculated quickly given its low runtime) can also be used as an initial heuristic for multi-objective flexible registration algorithms such as the BOFR-1.

As a perspective, an automatic method to align hole contours' vertices between CAD and SCAN is previewed to improve the metrological performance on hole localization defects. This alignment method could be based on barycentric coordinates regarding to the main border vertices.

Acknowledgments

The authors would like to thank the *French Ministry of National Education, Higher Education, and Research (MENESR)*, the *Region Auvergne-Rhone-Alpes (France) (via COOPERA Project GEOFLEX)*, and the *École de Technologie Supérieure (ÉTS, Canada)* for their financial contribution.

Bibliography

[1] G. N. Abenhaim, A. Desrochers, and A. Tahan, "Nonrigid parts' specification and inspection methods: Notions, challenges, and recent advancements," *International Journal of Advanced Manufacturing Technology*, vol. 63, no. 5–8, pp. 741–752, 2012.

[2] A. Aidibe and A. Tahan, "IDB-CTB: Inspection of deformable bodies using curvature estimation and Thompson-Biweight test," *International Journal of Advanced Manufacturing Technology*, pp. 1–15, 2014.

[3] K. Blaedel, D. Swift, A. Claudet, E. Kasper, and S. Patterson, "Metrology of NonRigid Objects (Tech.

Rep. UCRL-ID-146957 LLNL)," USA, 2002.

[4] A. Weckenmann and J. Weickmann, "Optical inspection of formed sheet metal parts applying fringe projection systems and virtual fixation," *Metrology and Measurement Systems*, vol. 13, no. 4, pp. 321–334, 2006.

[5] A. Weckenmann, J. Weickmann, and N. Petrovic, "Shortening of Inspection Processes by Virtual Reverse Deformation," in *4th international conference and exhibition on design and production of machines and dies/molds*, 2007, pp. 21–23.

[6] C. Lartigue, F. Thiebaut, P. Bourdet, and N. Anwer, "Dimensional Metrology of Flexible Parts, Identification of Geometrical Deviations from Optical Measurements," in *Advanced Mathematical and Computational Tools in Metrology VII*, 2006, pp. 196–203.

[7] A. Jaramillo, P. Boulanger, and F. Prieto, "Online 3D Inspection of Deformable Parts Using FEM Trained Radial Basis Functions," in *IEEE ICCV Workshops ICCV Workshops*, 2009, pp. 1733–1739.

[8] A. Jaramillo, F. Prieto, and P. Boulanger, "Fixtureless inspection of deformable parts using partial captures," *International Journal of Precision Engineering and Manufacturing*, vol. 14, no. 1, pp. 77–83, 2013.

[9] H. Radvar-Esfahlan and A. Tahan, "GNIF: Nonrigid Geometric Metrology using Generalized Numerical Inspection Fixtures," *Precision Engineering*, vol. 36, no. 1, pp. 1–9, 2012.

[10] H. Radvar-Esfahlan and A. Tahan, "RGNIF: Robust Generalized Numerical Inspection Fixture for the Metrology of Compliant Mechanical Parts," *The International Journal of Advanced Manufacturing Technology*, vol. 70, no. 5–8, pp. 1101–1112, 2014.

[11] V. Sabri, A. Tahan, X. T. Pham, D. Moreau, and S. Galibois, "Fixtureless profile inspection of non-rigid parts using the numerical inspection fixture with improved definition of displacement boundary conditions," *International Journal of Advanced Manufacturing Technology*, vol. 82, no. 5–8, pp. 1343–1352, 2016.

[12] S. Sattarpanah Karganroudi, J. C. Cuilliere, V. Francois, and A. Tahan, "Automatic fixtureless inspection of non-rigid parts based on filtering registration points," *The International Journal of Advanced Manufacturing Technology*, vol. 87, no. 1–4, pp. 687–712, 2016.

[13] F. Thiebaut, C. Lacroix, L. Andolfatto, and C. Lartigue, "Evaluation of the shape deviation of non rigid parts from optical measurements," *International Journal of Advanced Manufacturing Technology*, vol. 88, no. 5–8, pp. 1937–1944, 2016.

[14] V. Sabri, G. N. Abenhaim, A. Tahan, and X. T. Pham, "A Method for Dimensional Metrology of Non-rigid Parts based on Arc Length Measurement at Free-state Condition," *International Journal of Advanced Manufacturing Technology*, 2017.

[15] V. Sabri, S. Sattarpanah Karganroudi, A. Tahan, J. C. Cuilliere, V. Francois, and X. T. Pham, "A Robust and Automated FE-based Method for Fixtureless Dimensional Metrology of Non- rigid Parts using an Improved ...," *The International Journal of Advanced Manufacturing Technology*, no. February, 2017.

[15] A. Aidibe and A. Tahan, "IDB-ACPD: Adapting the coherent point drift algorithm to the fixtureless dimensional inspection of compliant parts," *The International Journal of Advanced Manufacturing Technology*, 2015.

[17] K. Babanezhad, G. Foucault, A. Tahan, and J. Bigeon, "BOFR-1: A Bi-Criterion Flexible Registration Method for Fixtureless Inspection of Compliant Parts," *Procedia CIRP Journal*, vol. 46, pp. 307–310, 2016.

[18] G. N. Abenhaim, A. Tahan, A. Desrochers, and R. Maranzana, "IDI: A Novel Approach for the Inspection of Flexible Parts without the Use of Special Fixtures," *Journal of Manufacturing Science and Engineering*, vol. 133, no. 1, p. 11009, 2011.

[19] R. Thompson, "A Note on Restricted Maximum Likelihood Estimation with an Alternative Outlier Model," *Journal of the Royal Statistical Society. Series B (Methodological)*, vol. 47, no. 1, pp. 53–55,

1985.

[20] D. C. Hoaglin, F. Mosteller, and J. W. Tukey, *Understanding Robust and Exploratory Data Analysis*, 1st ed. Wiley-Interscience, 2000.

[21] J. A. Sethian, "A Fast Marching Level Set Method for monotically advancing fronts," *Proceedings of the National Academy of Sciences*, vol. 93, no. 4, pp. 1591–1595, 1995.

[22] M. Mounaud, F. Thiebaut, P. Bourdet, H. Falgarone, and N. Chevassus, "Assembly sequence influence on geometric deviations propagation of compliant parts," *International Journal of Production Research*, vol. 49, no. 4, pp. 1021–1043, 2011.

[23] I. Gentilini and K. Shimada, "Predicting and evaluating the post-assembly shape of thin-walled components via 3D laser digitization and FEA simulation of the assembly process," *CAD Computer Aided Design*, vol. 43, no. 3, pp. 316–328, 2011.

[24] G. N. Abenhaim, A. Desrochers, A. Tahan, and J. Bigeon, "A Finite-Element Boundary Condition Setting Method for the Virtual Mounting of Compliant Components_slides," *Journal of Computing and Information Science in Engineering*, vol. 15, no. 4, p. 41005, 2015.

[25] P. J. Besl and H. D. McKay, "A method for registration of 3-D shapes," *IEEE Transactions on Pattern Analysis and Machine Intelligence*, vol. 14, no. 2, pp. 239–256, 1992.

[26] B. Delaunay, "Sur la sphère vide (Delaunay Triangulation)," *Bulletin de l'Académie des Sciences de l'URSS, Classe des sciences mathématiques et naturelles*, no. 6, pp. 793–800, 1934.

[27] J. B. Boisvert, "On the Use of Fast Marching Algorithms for Shortest Path Distance Calculation (Tech. Rep. CCG Annual 12 - P113)," Centre for Computational Geostatistics, Edmonton, Canada, 2010.

[28] K. Zuse, "Der Plankalkul (Konrad Zuse Internet Archive, ZIA-ID-0020, in German)," 1972.

[29] T. H. Cormen, C. E. Leiserson, R. L. Riverst, and C. Stein, *Introduction to Algorithms*, 2nd ed., vol. 53, no. 9. The MIT Press, 2001.

[30] F. E. Grubbs, "Sample Criteria for Testing Outlying Observations," *The Annals of Mathematical Statistics*, vol. 21, no. 1, pp. 27–58, 1950.

[31] B. Rosner, "Percentage Points for a Generalized ESD Many-outlier Procedure," *Technometrics*, vol. 25, no. 2, pp. 165–172, 1983.

[32] Automotive Industry Action Group (AIAG) (2010). Measurement Systems Analysis Reference Manual, 4th Edition. Chrysler, Ford, General Motors Supplier Quality Requirements Task Force.

[33] Suelí Fischer Beckert, Wagner Saucedo Paim, Critical analysis of the acceptance criteria used in measurementsystems evaluation, Int. J. Metrol. Qual. Eng., 8, 23 (2017)